Table VI. Average Bond Lengths (Å) Found in Several Lutetium Diphthalocyanine Complexes and in the Phthalocyanine Ligands of Typical Metallophthalocyanines, $Si(Pc)(OSi(CH_3)_3)_2$, and H_2Pc

	$[LuPc_2]^-$ (2^-)	$[LuHPc_2]$ (3)	$[LuPc_2]^c$	mean M(Pc)[d]	$Si(Pc)(OSiMe_3)_2$[d]	H_2Pc^e
Lu–Np (A)[a]	2.374 (2)	2.366 (4)	2.387 (4)			
Lu–Np (B)	2.392 (2)	2.376 (4)	2.372 (3)			
⟨Lu–Np⟩	2.383 (1)	2.371 (3)	2.380 (2)			
$Lu\cdots 4N_{iso}(A)$[a]	1.334	1.337	1.350			
$Lu\cdots 4N_{iso}(B)$	1.367	1.339	1.341			
$4N_{iso}(A)\cdots 4N_{iso}(B)$	2.701	2.676	2.691			
$N_{iso}–C_\alpha$[b]	1.370 (1)	1.373 (3)	1.376 (3)	1.377 (10)	1.375 (4)	1.37
$C_\alpha–C_\beta$[b]	1.459 (1)	1.463 (3)	1.456 (2)	1.453 (3)	1.449 (3)	1.47
$C_\beta–C_\beta$	1.391 (2)	1.390 (5)	1.390 (4)	1.394 (4)	1.386 (5)	1.41
$N_m–C_\alpha$[b]	1.328 (1)	1.329 (3)	1.327 (2)	1.326 (7)	1.321 (4)	1.30
$C_{Ph}–C_{Ph}$[b]	1.386 (1)	1.386 (2)	1.389 (3)	1.390 (4)	1.383 (8)	1.40

[a] N_p denotes the centroid of the four isoindole nitrogens. [b] See Table IV for definition of N_{iso}, C_α, C_β, N_m, and C_{Ph}. [c] Data of ref 5. [d] Data of ref 17. [e] Data of ref 18.

2.372 (3) to 2.407 (3) Å (mean value 2.392 (2) Å)[16] with the isoindole nitrogens of ring B. In contrast, no such dissymmetry appears in the structure of $[LuHPc_2]$, where the lutetium atom lies 1.337 Å away from ring A and 1.339 Å out of ring B, the total separation between rings A and B being only 2.676 Å. Table V gives the dihedral angles between the mean planes of the pyrrole rings and phenyl rings with the corresponding $4N_{iso}$ mean planes of the phthalocyanine ligands. These ligands are severely distorted, but as usual the average bond distances and bond angles are not significantly different from those found in typical metallophthalocyanine[5,17] and H_2Pc[18] (Table VI).

The acidic hydrogen could not be located in the structure of $[LuHPc_2]$. The mean value of the $Lu–N_{iso}$ bond distances of 2.371 (3) Å is smaller than those found in $[LuPc_2]^-$ (2.383 (1) Å) and $[LuPc_2]$ (2.380 (2) Å). Thus, most probably the protonation does not take place at an isoindole nitrogen but at a methine nitrogen. In addition, the bond distances and angles found within the phthalocyanine ligands, which are not significantly different from those present in $[LuPc_2]^-$, $[LuPc_2]$,[5] typical metallophthalocyanine,[5,17] and $[H_2Pc]$[18] (Table VI), indicate that the protonated molecule must be completely disordered in the crystal. The slight dissymmetry which is present in the structure of the $[LuPc_2]^-$ ion in **2** and absent in $[LuHPc_2]$ (**3**) is most probably due to the cation–anion packing. The $[NBu_4]^+$ cations lie approximately over the phthalocyanine ring B. The electrostatic interactions between these groups lead to longer $Lu–N_{iso}(B)$ bond distances with respect to the $Lu–N_{iso}(A)$ bond lengths and to a slightly larger separation between the $4N_{iso}$ mean planes in $[LuPc_2]^-$ with respect to $[LuHPc_2]$ where the acidic hydrogen is completely delocalized over both phthalocyanine rings A and B. The bond distances and bond angles found in the cation $[NBu_4]^+$ and DMF molecules of solvation present in **2** show their usual values (Table IV).

Acknowledgment. We thank Professor J. S. Buchler, Institut für Anorganische Chemie, Technische Hochschule, Darmstadt, West Germany, for helpful discussions and Priv. Doz. Dr. M. Veith and M. Fischer (Technische Hochschule, Darmstadt, West Germany) for the mass spectrum.

Registry No. **1**, 112816-38-3; **2**, 112816-39-4; **2**·2DMF, 112839-63-1; **3**, 12369-74-3; $[LuPc_2]$, 79079-35-9; $[GdPc_2]$, 82800-45-1.

Supplementary Material Available: Tables SM-1 and SM-2 (anisotropic thermal parameters for all non-hydrogen atoms for **2** and **3**), Tables SM-3 and SM-4 (hydrogen atom parameters for **2** and **3**), Tables SM-5 and SM-6 (complete set of bond lengths for **2** and **3**), and Tables SM-7 and SM-8 (complete set of bond angles for **2** and **3**) (24 pages); Tables SM-9 and SM-10 (observed and calculated structure factors for all observed reflections (×10) for **2** and **3**) (53 pages). Ordering information is given on any current masthead page.

(17) Ciliberto, E.; Doris, K. A.; Pietro, W. J.; Reisner, G. M.; Ellis, E.; Fragala, I.; Herbstein, F. H.; Ratner, M. A.; Marks, T. I. *J. Am. Chem. Soc.* **1984**, *106*, 7748.
(18) Hoskins, B. F.; Mason, S. A. White, J. B. C. *J. Chem. Soc., Chem. Commum.* **1969**, 554.

Notes

Contribution from the Laboratoire de Chimie des Solides, UA CNRS No. 279, Université de Nantes, 2, rue de la Houssinière, 44072 Nantes Cedex 03, France

General Trends Observed in the Substituted Thiophosphate Family. Synthesis and Structure of $AgScP_2S_6$ and $CdFeP_2S_6$

Stephen Lee,[1] Pierre Colombet,* Guy Ouvrard, and Raymond Brec

Received September 23, 1987

The systematic study of a specific family of crystalline compounds can often reveal exciting trends in crystal structure chemistry. We report in this paper the synthesis and structure of $AgScP_2S_6$ and $CdFeP_2S_6$. The interest in these compounds is that they illustrate three points of general chemical interest: that metal superstructure is dependent on the oxidation state of the metals, that Ag(I) undergoes a distortion of its octahedral environment due to a suggested second-order Jahn–Teller effect, and that extended Hückel calculations together with a steric effect argument may help to explain the way in which metals order.

Experimental Section

Materials. Both $AgScP_2S_6$ and $CdFeP_2S_6$ were prepared in sealed quartz tubes from a stoichiometric mixture of the elements held at 600 °C for a 2-week period. In the case of $AgScP_2S_6$ the mixture was first left at a lower temperature (450 °C) to avoid any reaction with the quartz tube. The solid solution $Cd_xFe_{1-x}PS_3$ (x = 0.20, 0.40, 0.60, 0.80) was also synthesized. The single crystals used for the X-ray analysis were selected from the sample mass.

X-ray Crystallographic Procedure. X-ray powder patterns were obtained from an Enraf-Nonius Guinier camera using Cu $K\alpha_1$ radiation. The photographs were calibrated with silicium (a = 5.430 88 Å) and the unit cell dimensions refined by least-squares fits of the data. The diffraction patterns indicate that $AgScP_2S_6$ and $Fe_xCd_{1-x}P_2S_6$ are isotypic to $AgInP_2S_6$[2] and $FePS_3$[3] (or $CdPS_3$), respectively. The powder data of

* To whom correspondence should be addressed.

(1) NATO postdoctoral fellow. Current address: Department of Chemistry, University of Michigan, Ann Arbor, MI 48109.

0020-1669/88/1327-1291$01.50/0

Table I. Observed and Calculated Powder Data for $AgScP_2S_6$[a]

d^{obsd}, Å	d^{calcd}, Å	*hkl*	$100I/I_0$	d^{obsd}, Å	d^{calcd}, Å	*hkl*	$100I/I_0$
6.449	6.449	002	73.1	1.7817	1.7822	300	27.8
5.349	5.347	100	4.7	1.7640	1.7640	116	11.4
4.946	4.939	101	6.1	1.7406	1.7419	107	4.3
4.116	4.116	102	2.5	1.7179	1.7178	302	8.7
3.352	3.350	103	31.8	1.6127	1.6121	008	4.2
3.225	3.224	004	3.4	1.5903	1.5907	$21\bar{5}$	9.0
3.087	3.087	110	14.1	1.5592	1.5598	304	1.6
2.786	2.784	$11\bar{2}$	100	1.5438	1.5434	220	1.6
2.766	2.761	104	0.1	1.5161	1.5170	207	5.5
2.671	2.673	200	2.3	1.4999	1.5010	222	11.0
2.617	2.618	201	6.8	1.4729	1.4731	311	0.8
2.4707	2.4695	202	0.4		1.4723	216	0.7
2.3230	2.3232	105	20.0	1.4455	1.4451	$31\bar{2}$	0.4
2.2700	2.2701	203	2.7	1.4015	1.4018	$31\bar{3}$	4.8
2.2302	2.2297	114	34.8	1.3921	1.3921	$22\bar{4}$	5.3
2.1488	2.1495	006	1.5	1.3716	1.3719	306	1.3
2.0575	2.0579	204	0.7	1.3613	1.3615	$21\bar{7}$	5.0
2.0209	2.0208	210	0.6	1.2863	1.2856	315	6.8
1.9951	1.9964	121	3.2	1.2760	1.2764	403	1.8
	1.9944	106	0.5	1.2536	1.2537	$22\bar{6}$	3.2
1.8549	1.8562	205	0.49	1.2265	1.2266	320	0.4
1.8291	1.8288	123	6.3				

[a] The intensities are calculated by using the Lazy Pulverix program.

Table II. Cell Parameters of $Cd_xFe_{1-x}PS_3$

x	*a*, Å	*b*, Å	*c*, Å	*β*, deg	*V*, Å^3
0.00	5.947 (1)	10.300 (1)	6.722 (1)	107.16 (1)	393.3 (2)
0.20	5.997 (1)	10.388 (1)	6.758 (1)	107.20 (1)	402.1 (2)
0.40	6.055 (2)	10.485 (3)	6.791 (2)	107.26 (3)	411.7 (5)
0.60	6.109 (2)	10.610 (1)	6.811 (4)	107.28 (4)	421.8 (8)
0.80	6.168 (1)	10.678 (2)	6.845 (2)	107.34 (2)	430.3 (4)
1.00	6.218 (1)	10.763 (2)	6.867 (1)	107.58 (1)	438.1 (2)

Table III. Summary of Crystal Structure Determination for $AgScP_2S_6$ and $CdFeP_2S_6$[a]

	$AgScP_2P_6$	$CdFeP_2S_6$
color	reddish	black
cryst dimens, mm	0.25 × 0.20 × 0.02	
space group	$P\bar{3}1c$	$C2/m$
cell dimens (at 20 °C)		
a, Å	6.1736 (6)	6.080 (2)
b, Å	6.1736	10.478 (4)
c, Å	12.897 (2)	6.801 (3)
β, deg	90	107.26 (4)
V, Å^3	425.7 (2)	413.8 (4)
Z	2	2
fw	407.16	422.58
calcd density, g/cm^3	3.176	3.392
linear abs coeff, cm^{-1}	47.83	60.71
no. of unique intens with $F > 3.0\sigma(F)$	208	626
no. of variables	18	29
final residuals R, R_w	0.034, 0.043	0.033, 0.041
max Δ/σ for last cycle	0.00	0.00

[a] The cell dimensions are refined from powder data. $CdFeP_2S_6$ has not been corrected for absorption.

the scandium-containing compound are shown in Table I. The cell parameters of the $Cd_xFe_{1-x}PS_3$ solid solution are reported in Table II.

X-ray Weissenberg photographs (Nonius chamber) of single crystals of the studied compounds confirmed both of these isomorphisms. Intensity data were collected with an automated four-circle diffractometer (Enraf-Nonius CAD-4) working with graphite-monochromated Mo Kα radiation and θ–2θ scans (angle range of θ: 1.5–30°). The cell parameters of the single crystals (25 reflections were used for the refinements for each of the two structures) were within the experimental error of the cell parameters found by Guinier powder techniques. The crystal structure refinements were carried out by using the SDP-PLUS package (1982 version) distributed by Enraf-Nonius and written by Frenz.[4] An absorption correction was made for $AgScP_2S_6$. The two structures could be solved very satisfactorily by assuming the above-mentioned isomorphisms. The highest peaks in the final difference Fourier maps had heights of 0.75 and 0.53 e Å^{-3} for $AgScP_2P_6$ and $CdFeP_2S_6$, respectively. Crystal and data collection information is summarized in Table III. Final positions, thermal parameters, and main interatomic distances are listed in Tables IV and V. Additional details are available as supplementary material.

Table IV. Positional and Thermal Parameters and Their Estimated Standard Deviations for $AgScP_2S_6$ and $CdFeP_2S_6$[a]

atom	*x*	*y*	*z*	B_{eq}, Å^2
Ag	0.667	0.333	0.250	3.81 (5)
Sc	0.0	0.0	0.250	1.07 (5)
P	0.333	0.667	0.1646 (3)	0.91 (4)
S	0.3053 (3)	0.3377 (4)	0.1211 (1)	1.21 (3)
Cd,Fe	0.0	0.33240 (7)	0.0	1.72 (1)
S1	0.7585 (3)	0.0	0.2498 (3)	1.53 (3)
S2	0.2442 (2)	0.1617 (1)	0.2521 (2)	1.56 (2)
P	0.0559 (3)	0.0	0.1692 (3)	1.12 (3)

[a] The isotropic equivalent thermal parameter (B_{eq}) is defined as $^4/_3\sum_i\sum_j\beta_{ij}\vec{a}_i\cdot\vec{a}_j$.

Table V. Main Distances (Å) in the Studied Compounds

	$AgScP_2S_6$		
Ag–S	2.793 (1)	Sc–S	2.595 (2)
P–S	2.029 (2)	P–P	2.203 (5)
	$CdFeP_2S_6$		
Cd,Fe–S_1	2.619 (1) (×2)	Cd,Fe–S_2	2.614 (1) (×2)
Cd,Fe–S_2	2.635 (1) (×2)	mean Cd,Fe–S	2.623
P–S_1	2.039 (2) (×1)	P–S_2	2.029 (1) (×2)
mean P–S	2.032	P–P	2.198 (4)

Results and Discussion

Both $AgScP_2S_6$ and $CdFeP_2S_6$ are thus variants of the $Fe_2P_2S_6$ structure type. They differ from each other in the way metals order: in $AgScP_2S_6$ the metals are ordered so that this compound contains a superstructure of $FePS_3$[5] while in $CdFeP_2S_6$ the metals are disordered, the compound showing no superstructure.[6] This difference is correlated with the fact that in $AgScP_2S_6$ the metals

(2) Ouili, Z.; Leblanc, A.; Colombet, P. *J. Solid State Chem.* **1987**, *66*, 86.
(3) Hahn, H.; Klingen, W.; Eulenberger, G. *Naturwissenshaften* **1970**, *57*, 88. Brec, R. *Solid State Ionics* **1986**, *22*, 3.
(4) Frenz, B. *Enraf-Nonius Structure Determination Package*; Delft University Press: Delft, The Netherlands, 1982.
(5) $AgScP_2S_6$ not only has a metal superstructure related to $FePS_3$ but also has the sulfur shifted from an fcc to an hcp arrangement.[2]
(6) The X-ray powder analysis shows (Table I) that the $Cd_xFe_{1-x}P_2S_6$ cell parameter evolution as a function of *x* follows Vegard's law. Such a behavior is in line with the random distribution of the metal sites of the MPS_3 structure deduced from the $CdFeP_2S_6$ single-crystal study.

Table VI. ABS_2 Superstructures of NaCl

$NaCrS_2$ Type Sulfides
$KCeS_2$, $KCrS_2$, $KDyS_2$, $KErS_2$, $KEuS_2$, $KGdS_2$, $KHoS_2$, $KLaS_2$, $KNdS_2$, $KPrS_2$, $KSmS_2$, $KTbS_2$, KYS_2, $KYbS_2$, $LiErS_2$, $LiHoS_2$, $LiScS_2$, $LiSnS_2$, $LiYbS_2$, $NaCrS_2$, $NaDyS_2$, $NaEuS_2$, $NaGaS_2$, $NaHoS_2$, $NaInS_2$, $NaNdS_2$, $NaScS_2$, $NaSnS_2$, $NaSmS_2$, $NaTiS_2$, $NaYS_2$, $NaYbS_2$, $RbCrS_2$, $RbBiS_2$, $RbSnS_2$, $TlDyS_2$, $TlErS_2$, $TlEuS_2$, $TlGdS_2$, $TlHoS_2$, $TlInS_2$, $TlTnS_2$, $TlYS_2$, $TlYbS_2$
$AgYbS_2$ Type Chalcogenides
$AgYbS_2$, $AgGdSe_2$, $AgTbSe_2$, $AgDySe_2$, $AgHoSe_2$

are in different oxidation states (Ag(I) and Sc(III)) while in $CdFeP_2S_6$ they are in the same oxidation state (Fe(II) and Cd(II)). Upon examining many known sulfide phases,[7] we find that this observation is general. For example, chalcopyrite, an ordered superstructure of sphalerite, is only known for $A^IB^{III}S_2$ systems.[8] Similarly, there are two known superstructures of the NaCl structure: $NaCrS_2$ and $AgYbS_2$.[9] Both of these superstructures are only found when the metals are of unequal oxidation state (see Table VI) and in total there are some 50 such phases. We know of no example of a ternary sulfide in which two metals with the same oxidation state occupy equivalent sites[10] in an ordered fashion whatever the charge/radius ratio may be.

The metals in both $AgScP_2S_6$ and $CdFeP_2S_6$ lie in octahedral sites. It may be seen (Table IV) that Ag exhibits an abnormally large thermal parameter, as in the various ABP_2S_6-substituted phases. Also, the Cu in $CuCrP_2S_6$[11] shows a similar tendency to move away from the center of the octahedra.[12] We believe the reason for this large thermal parameter is due to a second-order Jahn–Teller coupling between the filled silver e_g manifold and the empty s orbital. Although we come to this rationalization after the fact, nevertheless it is reasonable that we should see this effect only for Ag(I) and Cu(I). To the left of Ag in the periodic table, the s orbitals will be too high in energy, while to the right the d orbitals will be too low in energy for an effective d–s coupling. Furthermore, both Ag and Cu are in a low oxidation state. Higher oxidation states would tend to drive the d orbitals lower in energy relative to the s orbital.

In order to corroborate this suggestion, we have examined other sulfide phases where Ag(I) or Cu(I) atoms lie in octahedral or tetrahedral sites. In turning first to the chalcopyrites $AgGaS_2$, $CuGaS_2$, and $CuInS_2$, we observe there is a strong tetrahedral site distortion. This contrasts with their phosphide analogues $ZnSiP_2$, $CdSiP_2$, and $ZnGeP_2$ ($A^{II}B^{IV}P_2$ phases), which show little distortion.[8] The $NaCrS_2$ and $AgYbS_2$ structure types (in which the metals are octahedrally surrounded, as in the studied compounds) also are in accord with the second-order Jahn–Teller effect. It may be seen in Table VI that $NaCrS_2$ is the more prevalent of the two superstructures. The $AgYbS_2$ type is only found when Ag is one of the metals. This may be rationalized in the following manner: $NaCrS_2$ is a rhombohedral superstructure of NaCl while $AgYbS_2$ is a tetragonal one. We note

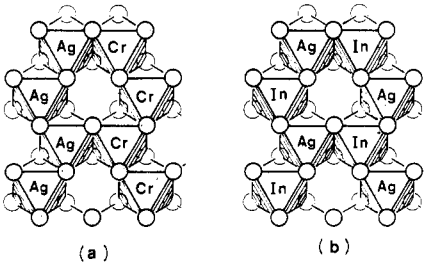

Figure 1. The two alternate superstructures of $FePS_3$: (a) the $AgCrP_2S_6$ superstructure adopted by $AgCrP_2S_6$ and $AgVP_2S_6$; (b) the $AgInP_2S_6$ superstructure adopted by $AgInP_2S_6$ and $AgScP_2S_6$. The figure shows one layer of the structure. The circles are sulfur atoms. Metal atoms fill the octahedra formed by the sulfurs. For the sake of clarity the phosphorus positions are left out. They lie in the unfilled, clear octahedra. All structures are layered, and therefore the third axis is not shown.

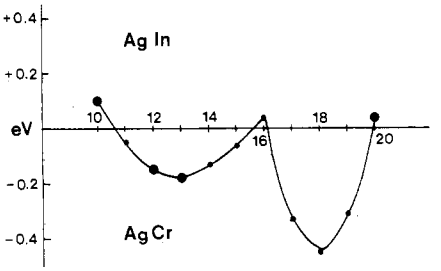

Figure 2. Extended Hückel calculation on the ABP_2S_6 system by the method in ref 14. The x axis gives the total A and B d-electron count (10 for $AgScP_2S_6$, 12 for $AgVP_2S_6$, 13 for $AgCrP_2S_6$, and 20 for $AgInP_2S_6$). The y axis plots the energy difference between the $AgInP_2S_6$ and the AgCr arrangements shown in Figure 1. The four known phases are represented by large filled circles. The extended Hückel calculation correctly predicts the superstructure for all four phases. Finally, the curve shows the difference in energy per orthorhombic unit cell.

that a distortion which keeps the 3-fold axis does not allow mixing between the e_g and s orbitals. Distortions which keep the 4-fold axis do allow such mixing. Indeed, the proposed structure for $AgYbS_2$ involves an approximate C_{4v} symmetry at the Ag site.

$AgScP_2S_6$ completes a series of compounds: $AgInP_2S_6$, $AgVP_2S_6$, and $AgCrP_2S_6$. All are ordered superstructures, but the last two phases have the same superstructure while $AgInP_2S_6$ and $AgScP_2S_6$ have another one (Figure 1). This well confirms experimentally the prediction of a simple extended Hückel type band calculation,[14] where the bonds involving the d electrons of the transition metals are taken into account (Figure 2). However, this band effect is small. For instance, the band calculations show an energy difference of only 0.1 eV/Cr atom for $AgCrP_2S_6$ between the two alternate superstructures.[15] Now, for those of the known ABP_2S_6 materials in which the assumed weak B(III)–B(III) bonding yields the occurrence of zigzag chains (Figure 1), it occurs that B(III) has a small ionic radius as compared to that of A(I).[2,17] Hence, another contribution to the driving force of the superstructure formation, based on a steric argument, has to be considered. The steric argument is as follows: when A(I) and B(III) of ABP_2S_6 are of highly disparate size, the superstructure that minimizes the amount of edge sharing between A(I) and B(III) octahedra will be adopted since such a configuration

(7) Villars, P.; Calvert, L. D. *Pearson's Handbook of Crystallographic Data for Intermetallic Phases*; American Society for Metals: Metals Park, OH, 1985.
(8) Abrahams, S. C.; Bernstein, J. L. *J. Chem. Phys.* **1973**, *59*, 5415 and references therein. Hall, S. R.; Stewart, J. M. *Acta Crystallogr., Sect. B: Struct. Crystallogr. Cryst. Chem.* **1973**, *B29*, 579.
(9) Julien-Pouzol, M.; Guittard, M. *C. R. Seances Acad. Sci., Ser. C.* **1969**, *269*, 316 and references therein.
(10) This does not preclude the metals from occupying inequivalent sites. An example of this is $BaNiS_2$, where Ba occupies a seven-coordinate site and Ni a five-coordinate one. Also, the converse statement is not true. The presence of metals of differing oxidation states does not ensure ordering.
(11) Colombet, P.; Leblanc, A.; Danot, M.; Rouxel, J. *J. Solid State Chem.* **1982**, *41*, 174.
(12) It should be noted that the large refined thermal ellipsoid for silver, which simulates static or dynamic displacements, can be an artifact for a subtle superstructure with ordered small Ag displacements. This point has already been discussed for $CuCrP_2S_6$,[11] in the case of Cu, and $AgCrP_2S_6$.[13] No superstructure leading to a significant lowering of the R factor could be found.
(13) Colombet, P.; Leblanc, A.; Danot, M.; Rouxel, J. *Nouv. J. Chim.* **1983**, *7*, 333.
(14) Lee, S. *J. Am. Chem. Soc.*, in press.
(15) (a) Recent high-resolution electron microscope results,[16] though, show a significant amount of disorder in $AgCrP_2S_6$, with the $AgScP_2S_6$ arrangement being one of the detected defects. This corresponds well with the slight energy difference of our calculations and may explain the difficulty of single-crystal selection. (b) More evidence which indicates that there is a band stabilization of Cr and V in the $AgCrP_2S_6$ systems is the contraction of the a parameter in the direction of the Cr and V chains.[16]
(16) Li, Z.; Dorignac, D.; Colombet, P.; Brec, R., submitted for publication in *J. Solid State Chem.*
(17) Lee, S.; Colombet, P.; Ouvrard, G.; Brec, R. *Mater. Res. Bull.* **1986**, *21*, 917.

minimizes the constraints. As the two metals become of more similar size, the system that minimizes the Madelung energy becomes preferable. In Figure 1, we show that the former arrangement is the $AgCrP_2S_6$ structure while the latter is the $AgInP_2S_6$ type. Thus, we see the larger Sc(III) cation leads to one structure, while the smaller V(III) and Cr(III) lead to the other.[15] Calculating the constraint energy difference between the two superstructures is a difficult task and has not yet been done. Consequently, it cannot be stated which out of the steric and band effects is the predominant one in determining the structure type in this series when the metals are of different oxidation state. They seem to be concomitant, and both explain the observed structures of the compounds synthesized so far.

Registry No. $AgScP_2S_6$, 113087-64-2; $CdFeP_2S_6$, 113087-65-3; Sc, 7440-20-2; Cd, 7440-43-9; Fe, 7439-89-6; P, 7723-14-0; S, 7704-34-9; $Cd_{0.2}Fe_{0.8}PS_3$, 113087-66-4; $Cd_{0.4}Fe_{0.6}PS_3$, 113087-69-7; $Cd_{0.6}Fe_{0.4}PS_3$, 113087-67-5; $Cd_{0.8}Fe_{0.2}PS_3$, 113087-68-6; $FePS_3$, 20642-11-9; $CdPS_3$, 28099-03-8; $AgVP_2S_6$, 105355-00-8; $AgCrP_2S_6$, 86745-59-7; $AgInP_2S_6$, 98319-31-4; Ag, 7440-22-4.

Supplementary Material Available: For the two structures, listings of anisotropic thermal parameters (1 page); listings of observed and calculated structure factors (6 pages). Ordering information is given on any current masthead page.

Contribution from the Department of Chemistry, University of San Francisco, San Francisco, California 94117

Evidence for a Specific Solvent–Solute Interaction as a Major Contributor to the Excited-State Distortion of the Emitting Charge-Transfer State in the Complex $(bpy)_2Ru^{II}(CN)_2$

Ella Y. Fung, Arthur C. M. Chua, and Jeff C. Curtis*

Received April 8, 1987

A recent paper from this laboratory presented evidence showing that specific solvent–solute interactions of a Lewis acid–base nature in the second coordination sphere of a ruthenium ammine complex could give rise to a significant contribution to the Franck–Condon barrier to optical electron transfer in a mixed-valence dimer such as the one shown here:[1]

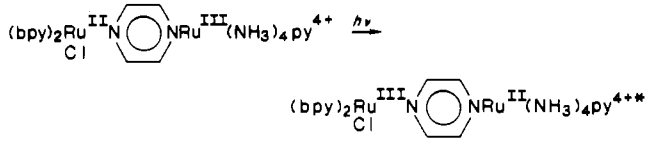

The origin of the effect in this molecule arises from the differential Lewis acidity of the ammine protons between the ground- and excited-state electronic distributions and the subsequent rearrangement of the hydrogen bonds in the secondary coordination sphere about the ammine moiety upon electron transfer.

We wish to report here a related observation concerning the $(bpy)_2Ru^{II}(CN)_2$ molecule. In this case the solute acts as a Lewis base and the solvent as a Lewis acid. The strength of this interaction depends on the electronic state of the solute. The ruthenium complex in its lowest lying metal-to-ligand-charge-transfer (MLCT) state has an electron largely transferred from the Ru(II) center out to one of the bpy rings.[2] The drop in electron density at the cyano nitrogens compared to the ground state is profound;

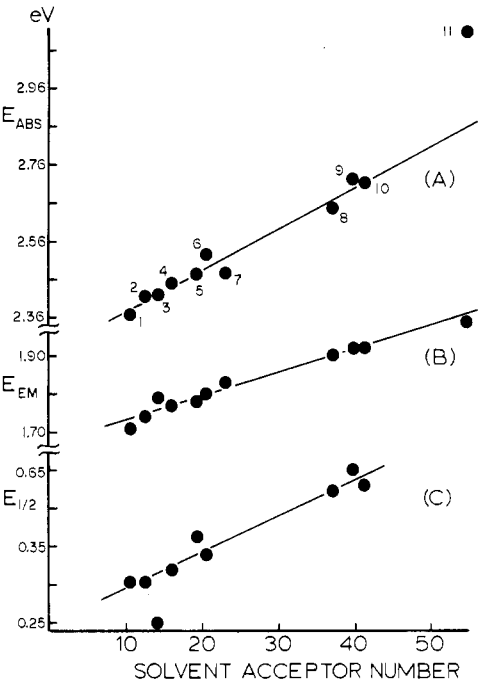

Figure 1. Dependences of (A) absorption band maximum, (B) emission band maximum, and (C) $Ru^{II/III}$ potential (fc/fc$^+$ reference) on solvent acceptor number.

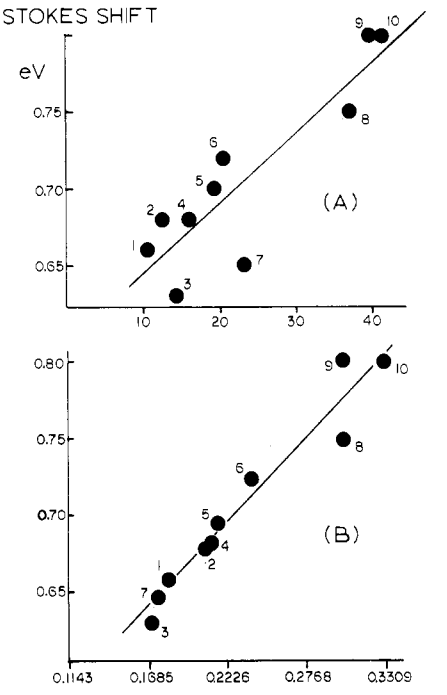

Figure 2. Dependence of Stokes shift on (A) solvent acceptor number and (B) composite function $X = 0.0038$(acceptor number) $+ 0.316(1/n^2 - 1/Ds)$.

for example, the K_a of the protonated complex has been shown to increase by nearly 6 orders of magnitude in the excited state relative to the ground state.[2b] This dramatic contrast in chemical nature between ground and excited states gives rise to a rather subtle manifestation if we investigate the charge-transfer absorption and emission spectra of the neutral molecule in a range of solvents with varying Lewis acidity. In this case we find that the Stokes shift exhibits a strong dependence on the strength of the specific solvent–solute interaction.

Results and Discussion

Table I lists the different solvents used along with their Gutmann acceptor numbers (a convenient measure of Lewis acidity),[3]

(1) De La Rosa, R.; Chang, P. S.; Salaymeh, F.; Curtis, J. C. *Inorg. Chem.* **1985**, *24*, 4229.
(2) (a) Demas, J. N.; Turner, T. F.; Crosby, G. A. *Inorg. Chem.* **1969**, *8*, 674. (b) Peterson, S. H.; Demas, J. N. *J. Am. Chem. Soc.* **1976**, *98*, 7880. (c) Peterson, S. H.; Demas, J. N. *J. Am. Chem. Soc.* **1979**, *101*, 6571. (d) Demas, J. N.; Peterson, S. H.; Harris, E. W. *J. Phys. Chem.* **1977**, *81*, 1039.

0020-1669/88/1327-1294$01.50/0